

Structure Factors for Hot Neutron Matter from *Ab Initio* Lattice Simulations with High-Fidelity Chiral Interactions

Yuan-Zhuo Ma,^{1,2} Zidu Lin,³ Bing-Nan Lu,⁴ Serdar Elhatisari,^{5,6} Dean Lee,²

Ning Li,⁷ Ulf-G. Meißner,^{6,8,9} Andrew W. Steiner,^{3,10} and Qian Wang¹

¹Key Laboratory of Atomic and Subatomic Structure and Quantum Control (MOE),
Institute of Quantum Matter, South China Normal University, Guangzhou 510006, China

²Facility for Rare Isotope Beams and Department of Physics and Astronomy, Michigan State University, MI 48824, USA

³Department of Physics and Astronomy, University of Tennessee Knoxville

⁴Graduate School of China Academy of Engineering Physics, Beijing 100193, China

⁵Faculty of Natural Sciences and Engineering, Gaziantep Islam Science and Technology University, Gaziantep 27010, Turkey

⁶Helmholtz-Institut für Strahlen- und Kernphysik and Bethe Center for Theoretical Physics, Universität Bonn, D-53115 Bonn, Germany

⁷School of Physics, Sun Yat-Sen University, Guangzhou 510275, China

⁸Institute for Advanced Simulation, Institut für Kernphysik,
and Jülich Center for Hadron Physics, Forschungszentrum Jülich, D-52425 Jülich, Germany

⁹Tbilisi State University, 0186 Tbilisi, Georgia

¹⁰Physics Division, Oak Ridge National Laboratory

We present the first *ab initio* lattice calculations of spin and density correlations in hot neutron matter using high-fidelity interactions at next-to-next-to-next-to-leading order (N3LO) in chiral effective field theory. These correlations have a large impact on neutrino heating and shock revival in core-collapse supernovae and are encapsulated in functions called structure factors. Unfortunately, calculations of structure factors using high-fidelity chiral interactions were well out of reach using existing computational methods. In this work, we solve the problem using a computational approach called the rank-one operator (RO) method. The RO method is a general technique with broad applications to simulations of fermionic many-body systems. It uses the fact that the determinant of a matrix composed of rank-one operators is at most linear in each operator coefficient. Using the RO method, we compute the vector and axial static structure factors for hot neutron matter as a function of temperature and density. The *ab initio* lattice results are in good agreement with virial expansion calculations at low densities and can be used to calibrate random phase approximation codes commonly used to estimate many-body effects on the neutrino opacity in core-collapse supernovae.

Introduction. Core-collapse supernovae (CCSNe) are catastrophic events heralding the death of massive stars. Under enormous gravitational pressure, the nickel-iron core converts to neutron-rich matter via inverse beta decay. This results in an infall of stellar matter followed by a violent rebound from the ultradense core. Meanwhile, copious numbers of neutrinos are produced. This neutrino flux provides energy to the shock wave and increases the likelihood of an explosion. Since the neutrino-nucleon scattering rates are greatly modified by the spin and density correlations in neutron-rich matter, understanding these correlations is important for modeling CCSNe explosions [1–4]. Early efforts in studying in-medium neutrino-nucleon scattering have used mean field methods such as the Hartree-Fock (HF) and random phase approximations (RPA) [5–8]. Extended virial expansions provide model-independent predictions in the limit of low densities and high temperatures [7–9].

More recently, *ab initio* lattice calculations of neutron matter and its structure factors were performed using pionless effective field theory at leading order, both in the limit of infinite scattering length [10] and at the physical scattering length [11]. These calculations are suitable for environments where the neutrons have momenta less than 100 MeV. We are using natural units where the speed of light, c , reduced Planck constant, \hbar , and Boltzmann constant, k_B , are set to unity. In order to describe neutron matter at densities and temperatures relevant for CCSNe, a good description of nucleons up to

300 MeV momenta is needed. The standard theoretical framework for this regime is provided by chiral effective field theory (χ EFT), where the forces mediated by the exchange of pions are treated explicitly [12, 13].

Recent advances in chiral effective field theory interactions and advanced quantum many-body methods have pushed forward the frontiers of *ab initio* nuclear calculations. Calculations are now possible for light nuclei [14–19], medium-mass [20–24], and heavy nuclei [25], as well as finite temperature systems [26–28]. In this work, we compute the spin and density correlations in neutron matter at various temperatures and densities using lattice chiral effective field theory at next-to-next-to-next-to leading order (N3LO). Such N3LO lattice calculations were previously not possible due to the large computational effort required. We therefore introduce a new computational approach called the rank-one operator (RO) method. A rank-one operator is an operator that can be expressed as an outer product of vectors, $|v_\alpha\rangle\langle v_\beta|$. The RO method uses the fact that the determinant of a matrix composed of rank-one operators is at most linear in the rank-one operator coefficients. It can be used with any Monte Carlo calculations of fermionic systems in nuclear physics, condensed matter, ultracold atomic gases, and quantum chemistry.

Methods. Nuclear lattice effective theory (NLEFT) is an *ab initio* method that combines effective field theory with lattice Monte Carlo (MC) simulations [14, 21, 26, 29–35]. The use of unrestricted Monte Carlo simulations allows for inves-

tigations of strong many-body correlations such as clustering [34, 36, 37]. Moreover, the pinhole trace algorithm [26] allows for *ab initio* calculations of nuclear thermodynamics.

For a fixed nucleon number N and at a given temperature T , the expectation value of an observable O in the canonical ensemble (CE) is given by

$$\langle O \rangle_N = \frac{Z_O(\beta, N)}{Z(\beta, N)} = \frac{\text{Tr}_N (e^{-\beta H} O)}{\text{Tr}_N (e^{-\beta H})}, \quad (1)$$

where $\beta = T^{-1}$ is the inverse of temperature, H is the Hamiltonian, and Tr_N is the trace over all the N -nucleon states. The canonical partition function $Z(\beta, N)$, can be written explicitly in the single-particle basis $c_i = (\mathbf{n}_i, \sigma_i, \tau_i)$ as

$$Z(\beta, N) = \sum_{c_1, \dots, c_N} \langle c_1, \dots, c_N | \exp(-\beta H) | c_1, \dots, c_N \rangle, \quad (2)$$

with \mathbf{n}_i an integer triplet specifying the lattice coordinates, σ_i is the spin, and τ_i is the isospin. To update and sum over initial/final states we implement the pinhole trace algorithm described in Ref. [26].

We use the auxiliary field formalism to rewrite $\exp(-\beta H)$ as a product of transfer matrices that depend on the auxiliary fields and pion fields [14, 30]. The transfer matrix $M(n_t)$ corresponds to the Euclidean time evolution at the time step, n_t . If we use L_t time steps, then we get a product of the form $M(L_t - 1) \cdots M(0)$, which upon integrating over auxiliary and pion fields gives $\exp(-\beta H)$. We use the shuttle algorithm described in Ref. [21] to update the auxiliary and pion fields.

It is also convenient to consider the partition function for the grand canonical ensemble (GCE),

$$\mathcal{Z}(\beta, \mu_G) = \sum_N e^{\beta \mu_G N} Z(\beta, N), \quad (3)$$

where μ_G is chemical potential. The expectation of an operator in the GCE can be evaluated as

$$\langle O \rangle_G = \frac{\sum_N \langle O \rangle_N e^{\beta \mu_G N} Z(\beta, N)}{\sum_N e^{\beta \mu_G N} Z(\beta, N)} = \sum_N \langle O \rangle_N w_N, \quad (4)$$

where w_N is the normalized neutron number probability. This distribution function w_N can be obtained by calculating CE partition function $Z(\beta, N) = e^{-\beta F(\beta, N)}$, where the free energy $F(\beta, N)$ is the integration of CE chemical potential $\mu(\beta, n)$ from an N_0 -particle system, $F(\beta, N) = F(\beta, N_0) + \int_{N_0}^N \mu(\beta, n) dn$. We use the Widom insertion method [26, 38, 39] to calculate CE chemical potential $\mu(\beta, n)$. Further details are presented in the Supplemental Material [40].

A primary challenge for NLEFT calculations is the Monte Carlo sign problem, caused by cancellations between positive and negative amplitudes. In order to mitigate this problem, we start from a simple interaction with no significant sign oscillations and use the perturbation theory to implement the difference between the simple interaction and the high-fidelity interaction. Perturbative calculations up to the second order correction in the energy have been implemented in lattice quantum Monte Carlo (QMC) simulations [35]. In this work we

perform calculations at first order only, however we greatly accelerate the convergence of perturbation theory using high-fidelity interactions generated using the method of wave function matching as described in Ref. [41].

We write each transfer matrix $M(n_t)$ as the sum of the simple-interaction transfer matrix $M^{(0)}(n_t)$ and the high-fidelity correction $M^{(1)}(n_t)$. At zeroth order in perturbation theory, we simply replace each $M(n_t)$ by $M^{(0)}(n_t)$, so that we have the product $M^{(0)}(L_t - 1) \cdots M^{(0)}(0)$. At first order in perturbation theory, we do the same process, but at time step n_t we use $M^{(1)}(n_t)$ instead of $M^{(0)}(n_t)$ and sum over n_t . Each simple-interaction transfer matrix $M^{(0)}(n_t)$ consists of the normal-ordered exponential of one-body operators. One-body operators have exactly one annihilation operator and one creation operator, and normal ordering refers to placing annihilation operators on the right and creation operators on the left. The amplitude

$$\langle c_1, \dots, c_N | M^{(0)}(L_t - 1) \cdots M^{(0)}(0) | c_1, \dots, c_N \rangle, \quad (5)$$

can be calculated quite easily by computing the determinant of the matrix of one-body amplitudes,

$$\mathcal{M}_{ij} = \langle c_i | M^{(0)}(L_t - 1) \cdots M^{(0)}(0) | c_j \rangle. \quad (6)$$

Calculating such amplitudes is significantly more challenging when there are operators acting on more than one particle. For our calculations of the structure factors, both the observable O and the corrections $M^{(1)}(n_t)$ are higher-body operators. The corresponding amplitudes can be calculated using Jacobi formulas for derivatives of matrix determinants [30]. However, the Jacobi formulas grow exponentially in complexity with the number of higher-body operators included and are not practical for calculations of higher-body observables using high-fidelity chiral interactions.

To address this problem, we introduce the rank-one operator (RO) method. Let us define the annihilation operator $F_\alpha = \sum_{\mathbf{n}} a_{i,j}(\mathbf{n}) f_{\alpha,i,j}(\mathbf{n})$ for a single-particle orbital function $f_{\alpha,i,j}(\mathbf{n})$ with i, j indicating the spin and isospin labels, respectively. The corresponding creation operator is $F_\alpha^\dagger = \sum_{\mathbf{n}} a_{\alpha,i,j}^\dagger(\mathbf{n}) f_{\alpha,i,j}^*(\mathbf{n})$. We note that $F_\alpha^\dagger F_\alpha$ is a one-body operator with rank one, and all higher powers of $F_\alpha^\dagger F_\alpha$ will vanish upon normal ordering. Then this yields the following useful relations,

$$F_{\alpha_1}^\dagger F_{\alpha_1} = \lim_{c_1 \rightarrow \infty} c_1^{-1} : \exp(c_1 F_{\alpha_1}^\dagger F_{\alpha_1}) : , \quad (7)$$

which can be easily extended to higher-body rank-one operators,

$$F_{\alpha_1}^\dagger F_{\alpha_1} F_{\alpha_2}^\dagger F_{\alpha_2} = \lim_{c_1, c_2 \rightarrow \infty} c_1^{-1} c_2^{-1} : \exp(c_1 F_{\alpha_1}^\dagger F_{\alpha_1} + c_2 F_{\alpha_2}^\dagger F_{\alpha_2}) : , \quad (8)$$

when the orbitals for α_1 and α_2 are orthogonal and the orbitals for α_1' and α_2' are orthogonal. This reduction to normal-ordered exponentials of one-body operators allows for very

efficient calculations of amplitudes without the factorial proliferation of terms as with the Jacobi formula.

Static structure factors are Fourier transforms of the fluctuations of the spin and density correlation functions. Let $\hat{\rho}$ and $\hat{\rho}_z$ be the particle density and spin density operators, respectively. Let ρ^0 be the average particle density and ρ_z^0 be the average spin density. Here we consider unpolarized neutron matter where ρ_z^0 equals zero. On the lattice, the vector and axial static structure factors can be written as

$$S_v(\mathbf{q}) = \frac{1}{L^3} \sum_{\mathbf{n}\mathbf{n}'} e^{-i\mathbf{q}\cdot\mathbf{n}} [\langle \hat{\rho}(\mathbf{n} + \mathbf{n}') \hat{\rho}(\mathbf{n}') \rangle - (\rho^0)^2],$$

$$S_a(\mathbf{q}) = \frac{1}{L^3} \sum_{\mathbf{n}\mathbf{n}'} e^{-i\mathbf{q}\cdot\mathbf{n}} [\langle \hat{\rho}_z(\mathbf{n} + \mathbf{n}') \hat{\rho}_z(\mathbf{n}') \rangle - (\rho_z^0)^2],$$
(9)

where \mathbf{n}, \mathbf{n}' represents coordinate on a L^3 cubic lattice. The expectation values of these two-body density correlation operators in Eq. (9) are calculated using the RO formalism. Further details can be found in Supplemental Materials [40].

Results. We perform simulations on $L^3 = 6^3, 7^3, 8^3$ cubic lattices with spatial lattice spacing $a = 1/150 \text{ MeV}^{-1} \approx 1.32 \text{ fm}$ and temporal lattice spacing $a_t = 1/1000 \text{ MeV}^{-1}$. Following the strategy in Ref. [26], we use average twisted boundary conditions to eliminate finite volume effects and accelerate the convergence to the thermodynamic limit. For twist angle θ_i along each spatial direction i , the possible lattice momenta are $2\pi n_i/L + \theta_i/L$, with some integer n_i . The averaging over all possible twist angles θ_i is done by Monte Carlo sampling.

In Fig. 1 we present NLEFT results in the GCE for the static structure factors S_v and S_a in the long wavelength limit, $q \rightarrow 0$. The results are calculated at a temperature of 20 MeV and plotted as a function of density. We show lattice results corresponding to the high-fidelity N3LO chiral interaction generated using wave function matching (WFM). With increasing density both S_v and S_a drop gradually but with different trends. The last data point for S_a at high density is omitted due to the large uncertainty. Corresponding results for the chemical potential, fugacity, density and pressure are listed in Table I. The uncertainties shown in the graphs and the table are stochastic errors only. We discuss systematic errors at the end of this section.

The virial expansion makes model-independent predictions for structure factors in hot and dilute nucleonic gas by encoding the elastic nucleon-nucleon scattering phase shifts into the 2nd order virial coefficients [8]. As the fugacity $z = \exp(\mu/T)$ gradually increases, the 2nd-order virial expansion loses its accuracy in predicting these structure factors. Consequently, the 2nd virial S_v and S_a are only presented when $z \leq 0.45$. By approximating the pure neutron matter as a unitary Fermi gas, where the scattering length is infinite and the interaction range is zero, the 4th order unitary virial expansion predicts the vector and axial structure factors in a wider range of densities [9]. We also carry out a mixed virial calculation to estimate the truncation error in the virial expansion, where the 2nd virial simulation is extended with the 3rd and the 4th

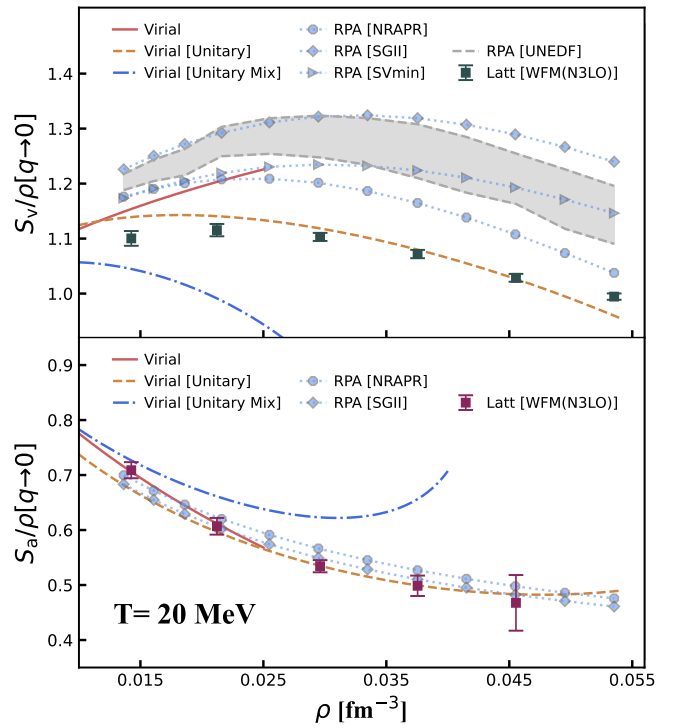


FIG. 1. Calculated static structure factors of S_v and S_a at the long-wavelength limit ($q \rightarrow 0$) with $T = 20 \text{ MeV}$. The red line is the virial expansion at 2nd order, the orange and the blue line represent the virial expansion at 4th order for unitary gas, and “Mix” means the unitary coefficients of the first two orders are replaced by that of the 2nd virial expansion. The RPA calculations are carried out with four different interactions (NRAPR, SGII, SVmin and UNEDF). WFM(N3LO) represents the NLEFT calculations with the wave function matching N3LO interaction.

order unitary virial coefficients.

For comparison, we also show in Fig. 1 results obtained using virial expansions and RPA calculations. The area in between the “Virial” and the “Unitary Mix” structure factors is a rough approximation of the truncation error of the virial expansion. Note that both S_v and S_a predicted by lattice calculations fall within this error band approximately and agree with the predictions by “Unitary” virial expansion quite well. This agreement with the unitary limit is unexpectedly good and may be benefiting from some fortuitous cancellation of different corrections. The RPA calculations provide self-consistent yet model-dependent calculations of structure factors not only for pure neutron matter but also for beta-equilibrium matter in a wide range of densities and temperatures [42]. In the vector current channel, we present the RPA S_v with NRAPR [43], SGII [44], SVmin [45] and UNEDF [46] Skyrme interactions. Note the UNEDF has quantified uncertainties of the Skyrme interactions, and we generate an error band of RPA S_v corresponding to these uncertainties. In the axial current channel, we present RPA calculations with NRAPR and SGII, in which the spin instability only appears at densities much higher than the saturation density ρ_0 . In both the vector and

TABLE I. Calculated grand canonical ensemble fugacity z , density ρ [fm^{-3}], pressure p [MeV/fm^3] with different chemical potential μ [MeV] at $T = 20$ MeV.

μ	-23.78	-16.58	-6.253	-2.592	0.6092
z	0.3045	0.4365	0.7315	0.8784	1.031
$\rho \times 100$	1.4274(4)	2.122(1)	3.754(1)	4.554(1)	5.353(1)
p	0.2458(1)	0.3618(1)	0.6307(2)	0.7768(2)	0.9305(2)

axial current channels, we note that the predictions of structure factors based on RPA calculations are satisfyingly close to the lattice calculations. The comparison between RPA and lattice calculations indicates the possibility of calibrating the Skyrme interactions as well as improving the RPA approach by NLEFT calculations in the future.

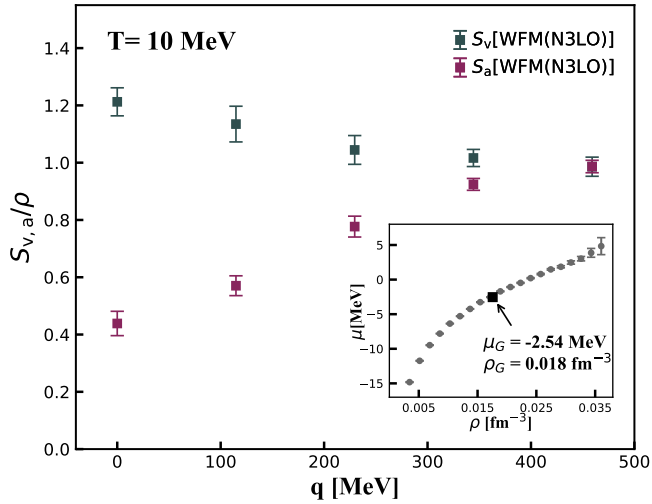


FIG. 2. Calculated momentum dependent neutron matter structure factors S_v and S_a at $T = 10$ MeV. WFM(N3LO) represents the NLEFT calculations with the wave function matching N3LO interaction. The insert figure shows calculated chemical potentials of CE systems which are used for the construction of GCE at the chemical potential $\mu_G = -2.54$ MeV and the density $\rho_G = 0.01758(4) \text{ fm}^{-3}$.

In Fig. 2, we present the momentum-dependent structure factor calculations at a temperature of 10 MeV in the GCE at density $\rho_G = 0.018 \text{ fm}^{-3}$. In the high momentum limit, both S_v and S_a go towards the system density. At long wavelengths, S_v and S_a have opposite trends. We also present the calculated chemical potentials of 20 CE systems in the inset of Fig. 2, which are used to construct this GCE system. We note that our results are similar to the unitary limit results presented in Ref. [10], although the results in Ref. [10] are at fugacity $z = 1.00$ and the results in Fig. 2 are at fugacity $z = 0.78$. The many-body corrections on the neutral current neutrino-nucleon interactions in CCSNe are usually estimated in the long wavelength limit, which is justified since the typical momentum transfer by scattered neutrinos is small compared to the thermal nucleon momentum $\sqrt{6MT}$, where M is

the nucleon mass. Note by applying exact dynamic structure factors in the calculation, the neutral current neutrino-nucleon scattering rates have small but noticeable deviations from the ones estimated in long wavelength limit [47]. Our *ab initio* calculations at finite momentum transfer provide benchmarks for the calculation of dynamic structure factors of pure neutron matter at finite temperatures.

We estimate an additional 5% systematic uncertainty for all of the lattice results presented in this work. The largest sources of systematic errors are due to finite system size errors, uncertainties in the nuclear interaction, and an approximation made in neglecting the numerically small higher-order corrections to the chemical potential, as discussed in the Supplemental Material. The finite system size error was obtained by analyzing the density and pressure with different box sizes. The errors due to uncertainties in the nuclear interaction and the neglected higher-order corrections to the chemical potential were performed by comparing results from calculations at different chiral orders in the canonical ensemble.

Summary. We have performed the first *ab initio* calculation of structure factors for hot neutron matter using high-fidelity chiral interactions at N3LO. The lattice results of vector and axial structure factors are in good agreement with virial expansions at low densities. The lattice predictions as a function of density, temperature, and momentum transfer can provide valuable benchmarks for calibrating RPA and other models commonly used in supernovae simulations. Further studies are planned to provide extensive benchmarking data for exactly this purpose.

We have introduced a new computational approach called the rank-one operator method to perform the calculations presented in this work. The rank-one operator method should have immediate applications to Monte Carlo simulations for nearly any quantum many-body systems composed of fermions. With new technologies such as wave function matching available to accelerate the convergence of perturbation theory, one has the possibility of avoiding Monte Carlo sign problems for a large class of fermionic many-body systems. The new computational paradigm requires computing amplitudes with multiple insertions of higher-body operators, and the rank-one operator method is ideally suited for this purpose.

Acknowledgement We are grateful for useful discussions with Chuck Horowitz, Gustav Jansen and members of the Nuclear Lattice Effective Field Theory Collaboration. This work has been supported by the Guangdong Major Project of Basic and Applied Basic Research No. 2020B0301030008, the National Natural Science Foundation of China under Grants No. 12105106, No. 12035007, China Postdoctoral Science Foundation under Grant No. BX20200136 and 2020M682747; ZL and AWS were supported by NSF PHY 21-16686. AWS was also supported by the Department of Energy Office of Nuclear Physics. DL was supported in part by the U.S. Department of Energy (DE-SC0021152, DE-SC0013365, DE-SC0023658, SciDAC-5 NUCLEI Collaboration). The work of UGM was supported by the European

Research Council (ERC) under the European Union’s Horizon 2020 research and innovation programme (grant agreement No. 101018170), by Deutsche Forschungsgemeinschaft (DFG, German Research Foundation) (project-ID 196253076 - TRR 110), the Chinese Academy of Sciences (CAS) President’s International Fellowship Initiative (PIFI) (Grant No. 2018DM0034), Volkswagen Stiftung (Grant No. 93562) and by the MKW NRW (funding code NW21-024-A). The work of QW was supported by Guangdong Provincial funding with Grant No. 2019QN01X172. Computational resources provided by the Oak Ridge Leadership Computing Facility through the INCITE award “Ab-initio nuclear structure and nuclear reactions”, the Southern Nuclear Science Computing Center, the Gauss Centre for Supercomputing e.V. (www.gauss-centre.eu) for computing time on the GCS Supercomputer JUWELS at the Jülich Supercomputing Centre (JSC), and the Institute for Cyber-Enabled Research at Michigan State University.

-
- [1] A. Mezzacappa, Annual Review of Nuclear and Particle Science **55**, 467 (2005), URL <https://doi.org/10.1146/annurev.nucl.55.090704.151608.1>
- [2] A. Burrows, S. Reddy, and T. A. Thompson, Nuclear Physics A **777**, 356 (2006), ISSN 0375-9474, special Issue on Nuclear Astrophysics, URL <https://www.sciencedirect.com/science/article/pii/S0375947404007730>.
- [3] A. Burrows, Rev. Mod. Phys. **85**, 245 (2013), URL <https://link.aps.org/doi/10.1103/RevModPhys.85.245>.
- [4] A. Burrows and D. Vartanyan, Nature **589**, 29 (2021), URL <https://www.nature.com/articles/s41586-020-03059-w.1>
- [5] R. F. Sawyer, Phys. Rev. C **40**, 865 (1989), URL <https://link.aps.org/doi/10.1103/PhysRevC.40.865.1>
- [6] S. Reddy, M. Prakash, J. M. Lattimer, and J. A. Pons, Phys. Rev. C **59**, 2888 (1999), URL <https://link.aps.org/doi/10.1103/PhysRevC.59.2888>.
- [7] C. Horowitz and A. Schwenk, Physics Letters B **642**, 326 (2006), ISSN 0370-2693, URL <https://www.sciencedirect.com/science/article/pii/S0370269306012081.1>
- [8] C. J. Horowitz, O. L. Caballero, Z. Lin, E. O’Connor, and A. Schwenk, Phys. Rev. C **95**, 025801 (2017), URL <https://link.aps.org/doi/10.1103/PhysRevC.95.025801.1,3>
- [9] Z. Lin and C. J. Horowitz, Phys. Rev. C **96**, 055804 (2017), URL <https://link.aps.org/doi/10.1103/PhysRevC.96.055804.1,3>
- [10] A. Alexandru, P. F. Bedaque, and N. C. Warrington, Phys. Rev. C **101**, 045805 (2020), URL <https://link.aps.org/doi/10.1103/PhysRevC.101.045805.1,4>
- [11] A. Alexandru, P. Bedaque, E. Berkowitz, and N. C. Warrington, Phys. Rev. Lett. **126**, 132701 (2021), URL <https://link.aps.org/doi/10.1103/PhysRevLett.126.132701.1>
- [12] E. Epelbaum, H.-W. Hammer, and U.-G. Meißner, Rev. Mod. Phys. **81**, 1773 (2009), 0811.1338, URL <https://link.aps.org/doi/10.1103/RevModPhys.81.1773.1>
- [13] R. Machleidt and D. R. Entem, Phys. Rept. **503**, 1 (2011), 1105.2919, URL <https://www.sciencedirect.com/science/article/pii/S0370157311000457.1>
- [14] D. Lee, Progress in Particle and Nuclear Physics **63**, 117 (2009), ISSN 0146-6410, URL <https://www.sciencedirect.com/science/article/pii/S014664100800094X.1,2>
- [15] E. Epelbaum, H. Krebs, T. A. Lähde, D. Lee, and U.-G. Meißner, Phys. Rev. Lett. **109**, 252501 (2012), URL <https://link.aps.org/doi/10.1103/PhysRevLett.109.252501>.
- [16] S. Pastore, A. Baroni, J. Carlson, S. Gandolfi, S. C. Pieper, R. Schiavilla, and R. B. Wiringa, Phys. Rev. C **97**, 022501 (2018), 1709.03592, URL <https://link.aps.org/doi/10.1103/PhysRevC.97.022501>.
- [17] B. R. Barrett, P. Navrátil, and J. P. Vary, Progress in Particle and Nuclear Physics **69**, 131 (2013), ISSN 0146-6410, URL <https://www.sciencedirect.com/science/article/pii/S0146641012001184>.
- [18] G. Hupin, S. Quaglioni, and P. Navrátil, Nature Commun. **10**, 351 (2019), 1803.11378, URL <https://doi.org/10.1038/s41467-018-08052-6>.
- [19] J. Carlson, S. Gandolfi, F. Pederiva, S. C. Pieper, R. Schiavilla, K. E. Schmidt, and R. B. Wiringa, Rev. Mod. Phys. **87**, 1067 (2015), URL <https://link.aps.org/doi/10.1103/RevModPhys.87.1067.1>
- [20] G. Hagen, T. Papenbrock, M. Hjorth-Jensen, and D. J. Dean, Reports on Progress in Physics **77**, 096302 (2014), URL <https://doi.org/10.1088/0034-4885/77/9/096302.1>
- [21] B.-N. Lu, N. Li, S. Elhatisari, D. Lee, E. Epelbaum, and U.-G. Meißner, Physics Letters B **797**, 134863 (2019), ISSN 0370-2693, URL <https://www.sciencedirect.com/science/article/pii/S0370269319305775.1,2>
- [22] V. Somà, C. Barbieri, T. Duguet, and P. Navrátil, Eur. Phys. J. A **57**, 135 (2021), 2009.01829, URL <https://doi.org/10.1140/epja/s10050-021-00437-4>.
- [23] R. Wirth, J. M. Yao, and H. Hergert, Phys. Rev. Lett. **127**, 242502 (2021), 2105.05415, URL <https://link.aps.org/doi/10.1103/PhysRevLett.127.242502>.
- [24] S. R. Stroberg, J. D. Holt, A. Schwenk, and J. Simonis, Phys. Rev. Lett. **126**, 022501 (2021), URL <https://link.aps.org/doi/10.1103/PhysRevLett.126.022501.1>
- [25] B. Hu et al., Nature Phys. **18**, 1196 (2022), 2112.01125, URL <https://doi.org/10.1038/s41567-022-01715-8.1>
- [26] B.-N. Lu, N. Li, S. Elhatisari, D. Lee, J. E. Drut, T. A. Lähde, E. Epelbaum, and U.-G. Meißner, Phys. Rev. Lett. **125**, 192502 (2020), URL <https://link.aps.org/doi/10.1103/PhysRevLett.125.192502.1,2,3>
- [27] J. Keller, C. Wellenhofer, K. Hebeler, and A. Schwenk, Phys. Rev. C **103**, 055806 (2021), 2011.05855, URL <https://link.aps.org/doi/10.1103/PhysRevC.103.055806>.
- [28] J. Keller, K. Hebeler, and A. Schwenk, Phys. Rev. Lett. **130**, 072701 (2023), 2204.14016, URL <https://link.aps.org/doi/10.1103/PhysRevLett.130.072701.1>
- [29] D. Lee, Phys. Rev. Lett. **98**, 182501 (2007), URL <https://link.aps.org/doi/10.1103/PhysRevLett.98.182501.1>
- [30] T. A. Lähde and U.-G. Meißner, *Nuclear Lattice Effective Field Theory: An introduction*, vol. 957 (Springer, 2019), ISBN 978-3-030-14187-5, 978-3-030-14189-9. 2

- [31] S. Elhatisari, D. Lee, G. Rupak, E. Epelbaum, H. Krebs, T. A. Lähde, T. Luu, and U.-G. Meißner, *Nature* **528**, 111 (2015), URL <http://www.nature.com/articles/nature16067>.
- [32] S. Elhatisari, N. Li, A. Rokash, J. M. Alarcón, D. Du, N. Klein, B.-n. Lu, U.-G. Meißner, E. Epelbaum, H. Krebs, et al., *Phys. Rev. Lett.* **117**, 132501 (2016), URL <https://link.aps.org/doi/10.1103/PhysRevLett.117.132501>.
- [33] N. Li, S. Elhatisari, E. Epelbaum, D. Lee, B.-N. Lu, and U.-G. Meißner, *Phys. Rev. C* **98**, 044002 (2018), URL <https://link.aps.org/doi/10.1103/PhysRevC.98.044002>.
- [34] S. Elhatisari, E. Epelbaum, H. Krebs, T. A. Lähde, D. Lee, N. Li, B.-n. Lu, U.-G. Meißner, and G. Rupak, *Phys. Rev. Lett.* **119**, 222505 (2017), URL <https://link.aps.org/doi/10.1103/PhysRevLett.119.222505>.
- [35] B.-N. Lu, N. Li, S. Elhatisari, Y.-Z. Ma, D. Lee, and U.-G. Meißner, *Phys. Rev. Lett.* **128**, 242501 (2022), URL <https://link.aps.org/doi/10.1103/PhysRevLett.128.242501>. 1, 2
- [36] N. Summerfield, B.-N. Lu, C. Plumberg, D. Lee, J. Noronha-Hostler, and A. Timmins, *Phys. Rev. C* **104**, L041901 (2021), URL <https://link.aps.org/doi/10.1103/PhysRevC.104.L041901>. 2
- [37] S. Shen, S. Elhatisari, T. A. Lähde, D. Lee, B.-N. Lu, and U.-G. Meißner, *Nature Commun.* **14**, 2777 (2023), 2202.13596, URL <https://doi.org/10.1038/s41467-023-38391-y>. 2
- [38] B. Widom, *The Journal of Chemical Physics* **39**, 2808 (1963), <https://doi.org/10.1063/1.1734110>, URL <https://doi.org/10.1063/1.1734110>. 2
- [39] K. Binder, *Reports on Progress in Physics* **60**, 487 (1997), URL <https://doi.org/10.1088/0034-4885/60/5/001>. 2
- [40] *Supplemental material*, URL <https://doi.org/10.1088/0034-4885/60/5/001>. 2, 3
- [41] S. Elhatisari, L. Bovermann, E. Epelbaum, D. Frame, F. Hildenbrand, M. Kim, Y. Kim, H. Krebs, T. A. Lähde, D. Lee, et al. (2022), 2210.17488, URL <https://doi.org/10.48550/arXiv.2210.17488>. 2
- [42] Z. Lin, A. W. Steiner, and J. Margueron, *Phys. Rev. C* **107**, 015804 (2023), 2207.05927, URL <https://link.aps.org/doi/10.1103/PhysRevC.107.015804>. 3
- [43] A. W. Steiner, M. Prakash, J. M. Lattimer, and P. J. Ellis, *Phys. Rept.* **411**, 325 (2005), nucl-th/0410066, URL <https://www.sciencedirect.com/science/article/pii/S0370157305001043>. 3
- [44] N. van Giai and H. Sagawa, *Phys. Lett. B* **106**, 379 (1981), URL <https://www.sciencedirect.com/science/article/pii/0370269381906468>. 3
- [45] P. G. Reinhard and W. Nazarewicz, *Phys. Rev. C* **81**, 051303 (2010), 1002.4140, URL <https://link.aps.org/doi/10.1103/PhysRevC.81.051303>. 3
- [46] J. D. McDonnell, N. Schunck, D. Higdon, J. Sarich, S. M. Wild, and W. Nazarewicz, *Phys. Rev. Lett.* **114**, 122501 (2015), 1501.03572, URL <https://link.aps.org/doi/10.1103/PhysRevLett.114.122501>. 3
- [47] P. F. Bedaque, S. Reddy, S. Sen, and N. C. Warrington, *Phys. Rev. C* **98**, 015802 (2018), 1801.07077, URL <https://link.aps.org/doi/10.1103/PhysRevC.98.015802>. 4

SUPPLEMENTAL MATERIAL

A. Wave function matching and χ EFT Hamiltonian

In our lattice calculations, we use wave function matching [1] and perturbation theory to mitigate the Monte Carlo “sign problem”. Starting from the high-fidelity χ EFT Hamiltonian H , wave function matching performs a unitary transformation to create a new high-fidelity Hamiltonian H' such that wave functions at short distances match that of a simple Hamiltonian H^S . This unitary transformation can provide a rapidly converging expansion in powers of the difference $H' - H^S$. It has been shown that a Hamiltonian with Wigner’s SU(4) symmetry will be positive definite and has no sign problem [2]. Thus, the simple Hamiltonian H^S can be constructed with approximate SU(4) symmetry, and the gap $H' - H^S$ can be filled by lattice perturbation theory.

We choose a leading-order χ EFT interaction for the simple Hamiltonian [1, 3],

$$H^S = K + \frac{1}{2} c_{\text{SU4}} \sum_{\mathbf{n}} : \tilde{\rho}^2(\mathbf{n}) : + V_{\text{OPE}}^{\Lambda_\pi}, \quad (\text{X.1})$$

where K is the kinetic term with nucleon mass $m = 938.92$ MeV and the $::$ symbols mean normal ordering. $\tilde{\rho}$ is the density operator for nucleons with local and non-local smearing,

$$\tilde{\rho}(\mathbf{n}) = \sum_{i,j=0,1} \tilde{a}_{i,j}^\dagger(\mathbf{n}) \tilde{a}_{i,j}(\mathbf{n}) + s_L \sum_{|\mathbf{n}-\mathbf{n}'|=1} \sum_{i,j=0,1} \tilde{a}_{i,j}^\dagger(\mathbf{n}') \tilde{a}_{i,j}(\mathbf{n}'). \quad (\text{X.2})$$

The non-locally smeared annihilation and creation operators, \tilde{a} and \tilde{a}^\dagger , with spin $i = 0, 1$ (up, down) and isospin $j = 0, 1$ (proton, neutron) indices are defined as,

$$\tilde{a}_{ij}(\mathbf{n}) = a_{ij}(\mathbf{n}) + s_{\text{NL}} \sum_{|\mathbf{n}'-\mathbf{n}|=1} a_{ij}(\mathbf{n}'). \quad (\text{X.3})$$

We use local smearing parameter $s_L = 0.07$ and non-local smearing parameter $s_{\text{NL}} = 0.5$.

In addition to the short-range SU(4) symmetric interaction, there is also the one-pion-exchange (OPE) potential appearing at the leading order,

$$V_{\text{OPE}}^{\Lambda_\pi} = -\frac{g_A^2}{8F_\pi^2} \sum_{\mathbf{n}', \mathbf{n}, S', S, I} : \rho_{S', I}(\mathbf{n}') f_{S', S}(\mathbf{n}' - \mathbf{n}) \rho_{S, I}(\mathbf{n}) :, \quad (\text{X.4})$$

$$V_{C_\pi}^{\Lambda_\pi} = -C_\pi \frac{g_A^2}{8F_\pi^2} \sum_{\mathbf{n}', \mathbf{n}, S, I} : \rho_{S, I}(\mathbf{n}') f^\pi(\mathbf{n}' - \mathbf{n}) \rho_{S, I}(\mathbf{n}) :, \quad (\text{X.5})$$

where C_π is defined as,

$$C_\pi = -\frac{\Lambda_\pi (\Lambda_\pi^2 - 2M_\pi^2) + 2\sqrt{\pi} M_\pi^3 \exp(M_\pi^2/\Lambda_\pi^2) \text{erfc}(M_\pi^2/\Lambda_\pi^2)}{3\Lambda_\pi^3}. \quad (\text{X.6})$$

We regularize the OPE potential by a Gaussian form factor in momentum space [4]. Here f^π is a local regulator in momentum space,

$$f^\pi(\mathbf{n}' - \mathbf{n}) = \frac{1}{L^3} \sum_{\mathbf{q}} e^{-i\mathbf{q} \cdot (\mathbf{n}' - \mathbf{n}) - (\mathbf{q}^2 + M_\pi^2)/\Lambda_\pi^2}, \quad (\text{X.7})$$

and $f_{S', S}$ is the locally-regulated pion correlation function,

$$f_{S', S}(\mathbf{n}' - \mathbf{n}) = \frac{1}{L^3} \sum_{\mathbf{q}} \frac{q_{S'} q_S e^{-i\mathbf{q} \cdot (\mathbf{n}' - \mathbf{n}) - (\mathbf{q}^2 + M_\pi^2)/\Lambda_\pi^2}}{\mathbf{q}^2 + M_\pi^2}, \quad (\text{X.8})$$

where L is the length of our cubic box and momentum components q_S on the lattice are integers multiplied by $2\pi/L$. Finally, $\rho_{S, I}$ is the spin- and isospin-dependent density operator for nucleons,

$$\begin{aligned} \rho_{S, I}(\mathbf{n}) &= \sum_{i, j, i', j'=0,1} \tilde{a}_{i, j}^\dagger(\mathbf{n}) [\sigma_S]_{ii'} [\sigma_I]_{jj'} \tilde{a}_{i', j'}(\mathbf{n}) \\ &+ s_L \sum_{|\mathbf{n}-\mathbf{n}'|=1} \sum_{i, j, i', j'=0,1} \tilde{a}_{i, j}^\dagger(\mathbf{n}') [\sigma_S]_{ii'} [\sigma_I]_{jj'} \tilde{a}_{i', j'}(\mathbf{n}'), \end{aligned} \quad (\text{X.9})$$

where σ_S are Pauli matrices in spin space and τ_I are Pauli matrices in isospin space.

In the equations above, $g_A = 1.287$ is the axial-vector coupling constant (corrected for the Goldberger-Treiman discrepancy), $F_\pi = 92.2$ MeV is the pion decay constants, and $M_\pi = 134.98$ MeV is the (neutral) pion mass. The interaction given in Eq. (X.5) is a counterterm introduced to remove the short-range singularity from the one-pion exchange potential. In the simple Hamiltonian, we set $\Lambda_\pi = 180$ MeV and $C_\pi = 0$, and we treat the difference $V_{\text{OPE}}^{\Lambda_\pi=300 \text{ MeV}} - V_{\text{OPE}}^{\Lambda_\pi=180 \text{ MeV}}$ and the OPEP counterterm $V_{C_\pi}^{\Lambda_\pi}$ in perturbation theory where $\Lambda_\pi = b_\pi^{-1/2}$. More details can be found in Refs. [1, 3, 5].

The high-fidelity χ EFT Hamiltonian at N³LO has the form,

$$H = K + V_{\text{OPE}}^{\Lambda_\pi} + V_{C_\pi}^{\Lambda_\pi} + V_{\text{Coul}} + V_{3N}^{\text{Q}^3} + V_{2N}^{\text{Q}^4} + W_{2N}^{\text{Q}^4} + V_{2N, \text{WFM}}^{\text{Q}^4} + W_{2N, \text{WFM}}^{\text{Q}^4} \quad (\text{X.10})$$

where V_{Coul} is the Coulomb potential, $V_{3N}^{\text{Q}^3}$ is the three-body potential, $V_{2N}^{\text{Q}^4}$ corresponds to the two-body short-range interactions at N3LO, $W_{2N}^{\text{Q}^4}$ gives the two-body Galilean invariance restoration (GIR) interactions at N³LO, $V_{2N, \text{WFM}}^{\text{Q}^4}$ is the wave function matching interaction, and $W_{2N, \text{WFM}}^{\text{Q}^4}$ is the GIR correction to the wave function matching interaction. It should be mentioned that the contribution from $W_{2N, \text{WFM}}^{\text{Q}^4}$ is negligible while the computational cost is large, and we do not include it in our neutron matter simulations. More details are discussed in the Supplemental Material of Ref. [1].

B. Rank-one operator method and Jacobi formula

The matrix representing single particle amplitudes in the absence of any observable operator is denoted as \mathcal{M} , whereas the matrix denoted as $\mathcal{M}(O)$ represents single particle amplitudes when the observable operator O is inserted. In the framework of NLEFT, one-body operator amplitudes are evaluated using

$$\begin{aligned} \det \mathcal{M}(O) &= \left. \frac{d \det \mathcal{M}(\exp(tO))}{dt} \right|_{t=0} \\ &= \det \mathcal{M}[\exp(tO)] \text{tr} \{ \mathcal{M}^{-1} \exp(tO) \mathcal{M}[O \exp(tO)] \} \Big|_{t=0} \\ &= \det \mathcal{M} \text{tr} [\mathcal{M}^{-1} \mathcal{M}(O)], \end{aligned} \quad (\text{X.11})$$

in which we used the Jacobi identity,

$$\frac{d}{dt} [\det A(t)] = \det A(t) \cdot \text{tr} [A^{-1}(t) \cdot \frac{d}{dt} A(t)]. \quad (\text{X.12})$$

For a normal-ordered two-body operator, $: O_\alpha O_\beta :$, we use normal-ordered exponential $: \exp\{\alpha O_\alpha + \beta O_\beta\} :$ and calculate derivatives with respect to α and β . The second-order Jacobi formula can be used,

$$\partial_\alpha \partial_\beta [\det A] = \det A [\text{tr} (A^{-1} \partial_\alpha A) \text{tr} (A^{-1} \partial_\beta A) - \text{tr} (A^{-1} \partial_\alpha A A^{-1} \partial_\beta A) + \text{tr} (A^{-1} \partial_\alpha \partial_\beta A)]. \quad (\text{X.13})$$

Unfortunately, the Jacobi formula will grow exponentially in complexity as more higher-body terms are included. In this work, we have a two-body operator for the structure factor observable as well as two- and three-body χ EFT operators from the perturbative insertions of the high-fidelity interaction. Due to the many terms generated by the Jacobi formula, these calculations cannot be performed with current computational resources using the Jacobi formula only. If we instead use numerical derivatives to calculate the operators, we also get exponential growth in the number of finite differences required. We will encounter these difficulties in perturbation calculations. The 1st-order perturbation of operator expectations can be written as,

$$\langle O \rangle^{\text{1st}} = \frac{\mathcal{M}_O^{(0)}}{\mathcal{M}^{(0)}} + \frac{\mathcal{M}_O^{(1)}}{\mathcal{M}^{(0)}} - \frac{\mathcal{M}_O^{(0)}}{\mathcal{M}^{(0)}} \frac{\mathcal{M}^{(1)}}{\mathcal{M}^{(0)}} + \mathcal{O}((\mathcal{M}^{(1)})^2), \quad (\text{X.14})$$

where $\mathcal{M}^{(0)}$ and $\mathcal{M}^{(1)}$ stand for the non-perturbative and the 1st-order perturbative amplitude respectively, and the subscript O stands for the operator insertion. Considering all the complicated two- and three-body operators in M_1 at N³LO and the wave function propagation between operator O and M_1 , calculating $\mathcal{M}_O^{(1)}$ using the Jacobi formula or the derivative method presents a formidable computational challenge.

The RO method provides several efficient options for calculating $\mathcal{M}_O^{(1)}$. For structure factor calculations, it can be used entirely by itself or it can be used in some combination of Jacobi formulas and/or numerical derivatives. Here we choose the option which combines the RO method and numerical derivative method for the two-body observable and use the Jacobi formula to handle the perturbative corrections from the high-fidelity interactions. As an example, let us consider the normal-ordered two-body density correlation function, $\langle : \hat{\rho}(\mathbf{n} + \mathbf{n}') \hat{\rho}(\mathbf{n}') : \rangle$. We treat $\hat{\rho}(\mathbf{n}')$ using the RO formalism and handle $\hat{\rho}(\mathbf{n} + \mathbf{n}')$ using numerical derivatives,

$$\mathcal{M}[: \hat{\rho}(\mathbf{n} + \mathbf{n}') \hat{\rho}(\mathbf{n}') :] = \lim_{\substack{\epsilon \rightarrow 0 \\ c \rightarrow \infty}} \sum_{ij} \frac{\mathcal{M}\{\exp[c\hat{\rho}_{ij}(\mathbf{n}') + \epsilon\hat{\rho}(\mathbf{n} + \mathbf{n}')]\} - \mathcal{M}\{\exp[c\hat{\rho}_{ij}(\mathbf{n}')]\}}{c\epsilon}. \quad (\text{X.15})$$

The treatment of the perturbative corrections to $\mathcal{M}\{\exp[c\hat{\rho}_{ij}(\mathbf{n}') + \epsilon\hat{\rho}(\mathbf{n} + \mathbf{n}')]\}$ and $\mathcal{M}\{\exp[c\hat{\rho}_{ij}(\mathbf{n}')]\}$ from the high-fidelity interactions are handled using Jacobi formulas.

C. Grand canonical ensemble benchmarks for a free Fermi gas

As noted in the main text, observables in the grand canonical ensemble (GCE) can be calculated using a series of canonical ensembles (CE) with a weight distribution $w_N = e^{\beta\mu_G N} \frac{Z(\beta, T)}{Z(\beta, \mu_G)}$. In the thermodynamic limit, w_N will have a Gaussian dependence near its maximum. We take the derivative of w_N with respect to N and obtain,

$$\begin{aligned} \frac{\partial}{\partial N} \omega_N &= \omega_N \frac{\partial}{\partial N} [\mu_G N \beta - \beta F(N)] \\ &= \omega_N \beta [\mu_G - \mu(N)]. \end{aligned} \quad (\text{X.16})$$

This means that the Gaussian function will have the maximum when $\mu_G = \mu(N)$, where $\mu(N)$ is the N -particle CE chemical potential. In our lattice calculation, the CE chemical potential is calculated using the Widom insertion method [6–8].

We can benchmark these calculations for a free Fermi gas of neutrons. In the grand canonical ensemble, the particle number of free Fermi gas can be obtained from the integral of the level density with the Fermi-Dirac distribution,

$$\int_0^\Lambda \frac{\rho(\epsilon)}{1 + e^{\beta(\epsilon - \mu)}} d\epsilon = N, \quad (\text{X.17})$$

where $\Lambda = (\pi/a)^2/(2m)$ is the energy cutoff imposed by the lattice spacing a [8]. Its level density can be obtained using

$$\rho(E) = \frac{dN}{dE} = \frac{1}{\pi^2 \hbar^3} mV \sqrt{2mE}. \quad (\text{X.18})$$

In Fig. X.1, we show the free neutron gas results for an $L^3 = 6^3$ lattice box at $T = 10$ MeV. The left panel shows the CE chemical potential at different densities and the inset shows the CE weight distribution for the GCE with $\mu_G = 17.8$ MeV. In the right panel, we show the expectation values of the GCE particle number and benchmark them against the analytical solution in Eq. (X.17). We find a nice agreement between calculated GCE particle numbers and that from the analytical solutions. The small deviation in the last few points can be resolved by including more CE systems.

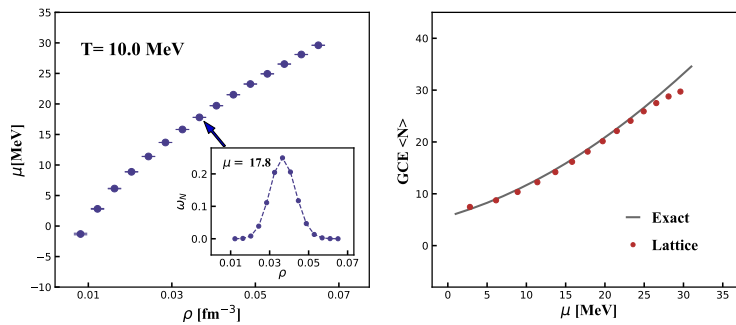


Figure X.1. Free Fermi gas chemical potentials are shown in the left panel. The insert figure shows the weight distribution w_N of CE systems for a GCE system at $\mu = 17.8$ MeV. The right panel shows the comparison of the calculated GCE particle number (red dots) and the analytical calculation (solid line).

D. Perturbation theory corrections to the static structure factors

To verify the corrections from the first-order perturbation theory to the structure factors, we perform lattice calculations with a simple Hamiltonian of the form

$$H = K + \frac{1}{2}c_{\text{SU4}} \sum_{\mathbf{n}} : \tilde{\rho}^2(\mathbf{n}) :, \quad (\text{X.19})$$

where K is the kinetic term. This simple Hamiltonian allows us to do fully non-perturbative lattice calculations without any sign oscillations. For our benchmark calculations, we introduce a parameter x that divides the original Hamiltonian H into a non-perturbative part (see also Ref. [9]),

$$H_0 = K + (1 - x) \times \frac{1}{2}c_{\text{SU4}} \sum_{\mathbf{n}} : \tilde{\rho}^2(\mathbf{n}) :, \quad (\text{X.20})$$

and a perturbative correction,

$$H_1 = x \times \frac{1}{2}c_{\text{SU4}} \sum_{\mathbf{n}} : \tilde{\rho}^2(\mathbf{n}) :. \quad (\text{X.21})$$

We note that for any value of x , $H = H_0 + H_1$, and the parameter x controls the size of the H_1 term.

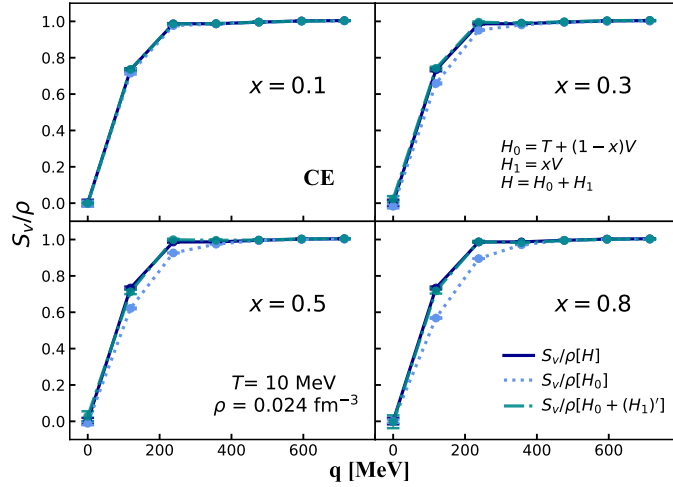


Figure X.2. Calculated CE static vector structure factor S_v with the full Hamiltonian H (solid line), with H_0 only (dotted line), and with $H_0 + H_1$ where H_1 is included at first-order in perturbation theory (dot-dashed line).

In Fig. X.2 and Fig. X.3, we show the momentum-dependence of S_v and S_a at $T = 10$ MeV in the canonical ensemble. The first-order perturbation theory calculation for S_v and S_a are benchmarked against results obtained with non-perturbative calculations using the full Hamiltonian $H = H_0 + H_1$. We see that S_v and S_a for H_0 (dotted lines) are diverging from the “full” Hamiltonian results (solid lines) as we increase x . Nevertheless, the perturbation theory results $S_{v/a}[H_0 + (H_1)']$ (dot-dashed lines) agree quite nicely with the “full” Hamiltonian results. For the axial structure factor, only a small discrepancy happens at $x = 0.8$ where H_0 is quite different from H .

E. Perturbation theory corrections to the chemical potential

We use the Widom insertion method [8] to compute differences in the free energy and calculate the chemical potential. In Table X.1 we show results at different orders in the chiral expansion at $T = 10$ MeV in the canonical ensemble for a range of densities. H^S corresponds to the Hamiltonian of Eq. X.1, which is used for non-perturbative calculations. Q^0 , Q^2 and Q^4 represents different orders in the χ EFT expansion. WFM(N3LO) includes wave function matching corrections at N3LO. It should be mentioned that H^S is similar to Q^0 which contains one-pion exchange and two S-wave contact interactions. However, to reduce the sign problem, H^S has a softer regulator for the one-pion exchange and does not include the counterterm of

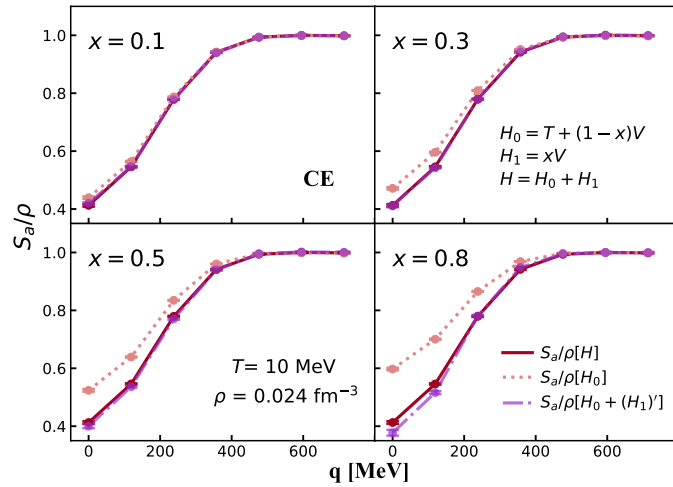


Figure X.3. Calculated CE static axial structure factor S_a , with the full Hamiltonian H (solid line), with H_0 only (dotted line), and with $H_0 + H_1$ where H_1 is included at first-order in perturbation theory (dot-dashed line).

Eq. (X.5). See Ref. [1] for more details. The differences between H^S and high-fidelity χ EFT interactions are treated in perturbation theory.

We observe that the chemical potentials at different orders in χ EFT along with non-perturbative H^S all agree with each other within stochastic error bars. This is most likely due to the fact that all of the interactions have approximately the same S-wave phase shifts. Given the negligible variation in the chemical potential from the perturbative corrections, we have simplified our lattice calculations by neglecting these small differences in the chemical potentials and using the H^S results.

Table X.1. Perturbation calculation of chemical potentials μ at $T = 10$ MeV. H^S corresponds to the Hamiltonian of Eq. X.1, which is used for non-perturbative calculations. Q^0 , Q^2 and Q^4 represents different order in the χ EFT expansion. WFM(N3LO) includes the corrections from wave function matching at N3LO, corresponding to Eq. X.10.

density [fm^{-3}]	H^S	Q^0	Q^2	Q^4	WFM(N3LO)
0.012	-4.732(24)	-4.706(24)	-4.709(24)	-4.715(24)	-4.717(24)
0.016	-2.626(25)	-2.593(25)	-2.595(25)	-2.605(25)	-2.609(25)
0.020	-0.953(26)	-0.911(26)	-0.916(26)	-0.929(26)	-0.934(26)
0.024	0.440(31)	0.485(31)	0.481(31)	0.460(31)	0.456(31)
0.028	1.708(39)	1.767(38)	1.762(38)	1.736(38)	1.744(39)
0.033	2.933(54)	2.992(54)	2.987(55)	2.953(56)	2.990(59)

F. RPA structure factors

In this subsection, we briefly summarize the needed formulas for calculating RPA $S_v(q)$ and $S_a(q)$. The dynamic vector (axial) structure factor of pure neutron matter based on RPA calculations is written as

$$S_{\text{RPA}}(q_0, q) = \frac{2 \text{Im}\Pi_{\text{RPA}}}{1 - \exp[-q_0/T]},$$

where q_0 is the transferred energy and q is the transferred momentum by scattered neutrinos. The Π_{RPA} is the polarization function of pure neutron matter, and is calculated given mean-field neutron matter polarization functions Π_0 ,

$$\Pi_{\text{RPA}} = \frac{\Pi_0}{1 - V_{\text{res}}\Pi_0}, \quad (\text{X.22})$$

where V_{res} is the (spin-dependent) residual interactions between neutrons. The detailed expression of Π_0 is provided in Ref. [10]. In vector current channel, $V_{\text{res}} = f_{nn}$. In axial current channel, $V_{\text{res}} = g_{nn}$. The f_{nn} and g_{nn} are Landau-Migdal parameters

and their detailed expression in terms of Skyrme parameters was carefully derived in Ref. [10]. Given the dynamic structure factor $S_{\text{RPA}}(q_0, q)$, we obtain the unitless static structure factor $S_{\text{RPA}}(q)$ from

$$S_{\text{RPA}}(q) = \frac{1}{2\pi n} \int S_{\text{RPA}}(q_0, q) dq_0, \quad (\text{X.23})$$

where n is the number density of pure neutron matter.

G. Virial structure factors

For the virial expansion up to the 4th order, the number density of pure neutron matter is written as

$$n = \frac{2}{\lambda^3} (z + 2z^2 b_2 + 3z^3 b_3 + 4z^4 b_4). \quad (\text{X.24})$$

The virial coefficients b_n for the unitary Fermi gas have been determined both theoretically and experimentally from ultracold gas experiments. We can use X.24 to obtain the fugacity z as a function of density. Given the fugacity, the unitary-limit virial static structure factors in long wavelength limit can be written as

$$S_v(q \rightarrow 0) = \frac{1 + 4zb_2 + 9z^2 b_3 + 16z^3 b_4}{1 + 2zb_2 + 3z^2 b_3 + 4z^3 b_4}, \quad (\text{X.25})$$

and

$$S_a(q \rightarrow 0) = \frac{1 + 4zb_2^0 + z^2(8b_3^0 + b_3) + z^3(16b_4^0 + 4b_{3,1})}{1 + 2zb_2 + 3z^2 b_3 + 4z^3 b_4}. \quad (\text{X.26})$$

The virial coefficients used in Eq. (X.25) and (X.26) are the same as in [11].

If we apply the virial expansion to realistic neutron matter up to 2nd order, we have

$$S_v(q \rightarrow 0) = 1 + \frac{1 + 4z^2 b_2}{\lambda^3 n}, \quad (\text{X.27})$$

and

$$S_a(q \rightarrow 0) = 1 + \frac{4}{\lambda^3} \frac{z^2 b_a}{n}, \quad (\text{X.28})$$

where $\lambda = \sqrt{2\pi/mT}$ is the thermal wavelength and the virial coefficients are extracted from nucleon-nucleon scattering phase shifts. The virial coefficients here are the same as those in [12]. Note that by setting the 3rd and the 4th order virial coefficients to zero, Eq. (X.25) and (X.26) reduce to Eq. (X.27) and Eq. (X.28).

-
- [1] S. Elhatisari, L. Bovermann, E. Epelbaum, D. Frame, F. Hildenbrand, M. Kim, Y. Kim, H. Krebs, T. A. Lähde, D. Lee, et al. (2022), 2210.17488, URL <https://doi.org/10.48550/arXiv.2210.17488>.
- [2] D. Lee, Phys. Rev. Lett. **98**, 182501 (2007), URL <https://link.aps.org/doi/10.1103/PhysRevLett.98.182501>.
- [3] B.-N. Lu, N. Li, S. Elhatisari, Y.-Z. Ma, D. Lee, and U.-G. Meißner, Phys. Rev. Lett. **128**, 242501 (2022), URL <https://link.aps.org/doi/10.1103/PhysRevLett.128.242501>.
- [4] P. Reinert, H. Krebs, and E. Epelbaum, Eur. Phys. J. A **54**, 86 (2018), ISSN 1434-6001, 1434-601X, URL <http://link.springer.com/10.1140/epja/i2018-12516-4>.
- [5] N. Li, S. Elhatisari, E. Epelbaum, D. Lee, B.-N. Lu, and U.-G. Meißner, Phys. Rev. C **98**, 044002 (2018), 1806.07994.
- [6] B. Widom, The Journal of Chemical Physics **39**, 2808 (1963), <https://doi.org/10.1063/1.1734110>, URL <https://doi.org/10.1063/1.1734110>.
- [7] K. Binder, Reports on Progress in Physics **60**, 487 (1997), URL <https://doi.org/10.1088/0034-4885/60/5/001>.
- [8] B.-N. Lu, N. Li, S. Elhatisari, D. Lee, J. E. Drut, T. A. Lähde, E. Epelbaum, and U.-G. Meißner, Phys. Rev. Lett. **125**, 192502 (2020), URL <https://link.aps.org/doi/10.1103/PhysRevLett.125.192502>.
- [9] T. A. Lähde, T. Luu, D. Lee, U.-G. Meißner, E. Epelbaum, H. Krebs, and G. Rupak, Eur. Phys. J. A **51**, 92 (2015), 1502.06787, URL <https://doi.org/10.1140/epja/i2015-15092-1>.
- [10] Z. Lin, A. W. Steiner, and J. Margueron, Phys. Rev. C **107**, 015804 (2023), 2207.05927, URL <https://link.aps.org/doi/10.1103/PhysRevC.107.015804>.
- [11] Z. Lin and C. J. Horowitz, Phys. Rev. C **96**, 055804 (2017), URL <https://link.aps.org/doi/10.1103/PhysRevC.96.055804>.
- [12] C. J. Horowitz, O. L. Caballero, Z. Lin, E. O'Connor, and A. Schwenk, Phys. Rev. C **95**, 025801 (2017), URL <https://link.aps.org/doi/10.1103/PhysRevC.95.025801>.